ECOSYSTEM PRODUCTIVITY AND THE GLOBAL CARBON CYCLE

A diverse set of publications arises from Ecosystem Productivity and the Global Carbon Cycle for 2002. Papers range from new physiologically based photosynthetic modeling, to ship surveys, to global decadal trends.

Behrenfeld et al. provide new parameterizations based on light acclimation and nutrients to improve primary production models, and also outline a summary of the analysis of global scale primary production.

In the Antarctic, Arrigo et al. documented the potential effects of an iceberg on ecosystem dynamics. They found the iceberg reduced primary production more than 40% below normal and altered the abundance and behavior of upper trophic level organisms.

Atkinson et al described ecosystem of physical dynamics in the coastal waters off Chile. Their observations utilized in situ sampling and satellite data to describe spatial variability in relation to upwelling, river runoff, intrusion of eddies, mixing and heating.

A longer set of cruise observations by Barlow et al in the Atlantic Ocean were used to characterize phytoplankton pigment characteristics. These pigments are indicative of ecosystem functionality, and indicated major changes across the various physical/biogeochemical regimes encountered in the greater North Atlantic.

Finally, Gregg and Conkright used a reanalysis of historical ocean color data to observe a six percent decline in global chlorophyll concentrations from the early 1980's to the present. Larger declines were observed at the high latitudes, while low latitudes indicated an increase. The changes have major implications for the global carbon cycle and climate change.

Ecological impact of a large Antarctic iceberg

Kevin R. Arrigo,[1] Gert L. van Dijken,[1] David G. Ainley,[2] Mark A. Fahnestock,[3] and Thorsten Markus[4]

Received 1 October 2001; accepted 20 December 2001; published 6 April 2002.

[1] Satellite imagery has been used to document for the first time the potential for large icebergs to substantially alter the dynamics of a marine ecosystem. The B-15 iceberg (~10,000 km^2), which calved off the Ross Ice Shelf in the biologically productive southwestern Ross Sea, Antarctica, restricted the normal drift of pack ice, resulting in heavier spring/summer pack ice cover than previously recorded. Extensive ice cover reduced both the area suitable for phytoplankton growth and the length of the algal growing season. Consequently, primary productivity throughout the region was >40% below normal, which changed both the abundance and behavior of upper trophic level organisms. *INDEX TERMS:* 1827 Hydrology: Glaciology (1863); 4207 Oceanography: General Arctic and Antarctic oceanography; 4275 Oceanography: General: Remote sensing and electromagnetic processes (0689)

1. Introduction

[2] Polar ice sheets and associated ice shelves are important indicators of climate change, responding to elevated temperatures with increased melt, accelerated motion, and/or increased iceberg calving [*Skvarca et al.*, 1999; *Scambos et al.*, 2000]. The calving of large tabular icebergs in the Antarctic has likely increased since the Last Glacial Maximum accompanying the formation of the Ross Ice Shelf [*Conway et al.*, 1999], with recent calving rates for large (>18.5 km) icebergs of 4.4 per year (iceberg tracking data obtained from the National Ice Center show that between 1978 and 2001, Antarctic ice sheets calved an average 4.4 icebergs larger than 18.5 km in length annually). Consequences of these calving events for marine ecosystems remain largely unexplored. Fortunately, the huge iceberg B-15 (at 295 km in length and up to 40 km in width is one of the largest icebergs ever observed), which calved off the Ross Ice Shelf in March 2000, is providing insights.

[3] The southwestern Ross Sea (Figure 1) is one of the most biologically productive regions of the Southern Ocean [*Smith and Gordon*, 1997; *Arrigo et al.*, 1998a]. Located on the Antarctic continental shelf, it owes its biological richness to the annual formation of the Ross Sea polynya, a region of diminished sea ice cover in the midst of heavy pack ice north of the Ross Ice Shelf. The Ross Sea polynya is formed by the strong, persistent katabatic winds that move sea ice offshore during winter, generally to the northwest [*Bromwich et al.*, 1992]. Come springtime, a large area of open water forms in this region as winds clear away the remaining sea ice. The resulting exposure of surface waters to sunlight is followed by a profuse growth of phytoplankton [*Arrigo et al.*, 1998b]. Concentrations of chlorophyll *a* (Chl *a*) in these blooms typically exceed 5 mg m^{-3} over an area of >100,000 km^2 (Figures 2a and 2b) [*Arrigo et al.*, 1998b; *Arrigo et al.*, 2000], compared to <0.05 mg m^{-3} in low productivity central ocean gyres. As a result of its high productivity, the Ross Sea supports large populations of upper-trophic level organisms, such as marine mammals and birds [*Ainley et al.*, 1984; *Kooyman and Burns*, 1999; *Kasamatsu et al.*, 1998]. Indeed, 25% and 30% of the world populations of the circumpolar Emperor (*Aptenodytes forsteri*) and Adélie penguins (*Pygoscelis adeliae*), respectively, nest at colonies in the Ross Sea [*Woehler*, 1993], which has a coastline <10% of the Antarctic continental margin.

2. Methods

[4] Sea ice distributions were computed from daily Special Sensor Microwave Imager (SSM/I) imagery obtained from the EOS Distributed Active Archive Center (DAAC) at the National Snow and Ice Data Center, University of Colorado, Boulder, CO. Images were processed to 6.25 km resolution using the algorithm of *Markus and Burns* [1995], and used to calculate open water areas. All satellite imagery were mapped to a common polar-stereographic projection using the Interactive Data Language (IDL, Research Systems, Inc.). Sea-viewing Wide Field-of-view Sensor (SeaWiFS) data were obtained from the Goddard Earth Sciences Data and Information Services Center, DAAC. Chl *a* concentrations were derived from SeaWiFS Level 2 data (4 km resolution) and processed using the NASA SeaDAS image processing software and OC4v4 algorithm. Validation studies for the Ross Sea show that SeaWiFS surface Chl *a* retrievals are within ±15% of in situ observations [*Arrigo et al.*, unpublished]. Multi-day (<1 week) Chl *a* composites were constructed to reduce loss due to cloud cover. Primary productivity was calculated from SeaWiFS data using the algorithm of *Arrigo et al.* [1998a]. Iceberg positions were projected using MODerate resolution Imaging Spectrometer (MODIS) band 1 (620–670 nm, 0.25 km resolution) imagery except for images where the sun was below the horizon; then the thermal infrared band 24 (4.433–4.498 μm, 1 km resolution) imagery were used. MODIS data were obtained from the Goddard Earth Sciences Data and Information Services Center, DAAC.

[5] At three penguin colonies on Ross Island (Cape Royds, Bird, and Crozier), stomach samples were taken from 3–5 adult penguins each week for five weeks, 25 December to ca. 22 January. Adults were forced to regurgitate stomach contents using the water-off loading technique: filling them with warm water, then turning them upside down in a plastic bucket.

3. Results and Discussion

[6] Satellite imagery from a variety of platforms show that on March 2000, the iceberg B-15 (iceberg numbers are assigned by the National Ice Center, Suitland, MD, USA) calved from the eastern portion of the Ross Ice Shelf (Figure 1). Almost immediately after calving, B-15 began to fragment, and at the present time, there are at least nine separate sections, denoted B-15A through B-15I, drifting in and around the western Ross Sea. By far the largest of these are B-15A and B-15B. Tracking the movement of the icebergs using imagery from MODIS shows that B-15A (~6,400 km^2) drifted westward along the front of the Ross Ice

[1]Department of Geophysics, Stanford University, Stanford, CA 94305-2215, USA.
[2]H. T. Harvey & Associates, San Jose, CA 95118, USA.
[3]ESSIC, University of Maryland, College Park, MD 20742-2465, USA.
[4]NASA Goddard Space Flight Center-University of Maryland Baltimore County Joint Center for Earth Systems Technology (NASA/GSFC-UMBC JCET), Greenbelt, MD 20771, USA.

0094-8276/02/2001GL014160$05.00

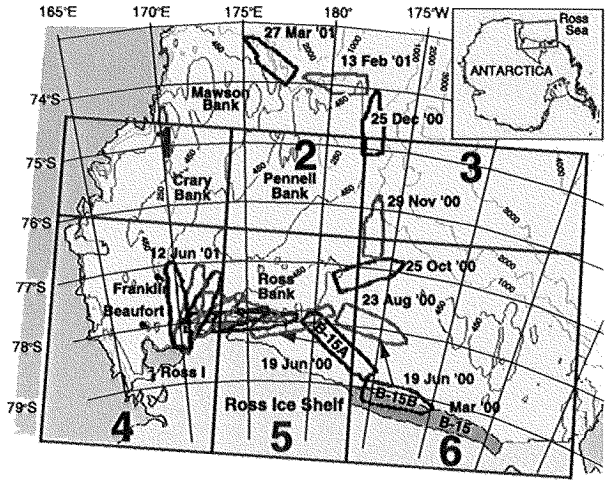

Figure 1. Map of the southwestern Ross Sea showing changes in the position of the B-15 iceberg and the location of the 6 regions referred to in the text. The sequential drift paths taken by B-15A and B-15B as determined from MODIS data are also shown. B-15A moved into its current position by edging past the Ross Bank but is now too large to move westward.

Shelf, likely guided by bathymetry and a narrow coastal current [*Keys et al.*, 1990] and is currently grounded near Ross Island at the face of the Ross Ice Shelf (Figure 1). B-15B first drifted to the north along the eastern edge of the Ross and Pennell banks and then moved west along the northern margin of the Pennell and Mawson Banks (Figure 1). It is now located near Cape Adare, over 1000 km from its original location. Like B-15A, however, other smaller icebergs (e.g. B-15C) remain grounded within the southwestern Ross Sea.

[7] In November 2000, nine months after the initial calving event, the pieces of B-15 were still in the southwestern Ross Sea, forming a barrier that greatly restricted the typical northwest drift pattern of pack ice (Figure 2c). As a result, sea ice concentrations measured using the SSM/I remained unusually heavy throughout November and early December 2000 (compare Figures 2a and 2b with 2c), the time when the southwestern Ross Sea normally shifts from being predominantly ice-covered to ice-free [*Arrigo et al.*, 2000]. As late as mid-December 2000, large amounts of sea ice remained piled up on the southeast side of the line of icebergs (Figure 2c), restricting the expansion of open water.

[8] Changes in the seasonal dynamics of sea ice cover brought about by the presence of B-15 are exemplified in an SSM/I time series for Region 5 (Figure 1), an area of the Ross Sea that was moderately impacted by B-15 (Figure 3a). During the spring of typical years (e.g. 1998–1999 and 1999–2000), sea ice cover in Region 5 diminishes rapidly, and from the beginning of December to early March, these waters are more than 80% ice-free. In contrast, the presence of the B-15 iceberg during 2000–2001 dramatically reduced the rate of ice advection, resulting in a 2-month delay in the time to reach maximum open water area. In fact, all regions of the southwestern Ross Sea experienced fewer days with <50% ice cover in 2000–2001, compared to the normal sea ice pattern represented by the 1998–2000 time period (Table 1). In the three regions adjacent to the Ross Ice Shelf (Figure 1), the number of days with sea ice concentrations below 50% was reduced by 37–48% in 2000–2001, and Region 3 did not become ice-free all year.

[9] The heavy sea ice conditions of 2000–2001 caused by the presence of the B-15 iceberg had a dramatic effect on phytoplankton populations throughout the southwestern Ross Sea. In ordinary years, phytoplankton begin to bloom in mid-November (Figure 3b), just as the area of open water and the availability of light begins to increase (Figure 3a). Imagery from the Sea-viewing Wide Field-of-view Sensor (SeaWiFS) shows that typically, Chl *a* concentrations in the Ross Sea increase rapidly, as do calculated rates of primary production (Figure 3c), eventually peaking in late December. After blooming for approximately six weeks, phytoplankton growth rates begin to diminish. At this time, loss processes such as grazing and sinking exceed rates of growth, causing Chl *a* abundance and primary production to decline steadily.

[10] SeaWiFS imagery reveals, however, that the normal phytoplankton dynamics in the Ross Sea were markedly altered during 2000–2001, most probably a direct result of the effects of the B-15 iceberg. Diminished light availability due to the high concentrations of sea ice present throughout the southwestern Ross Sea in the austral spring and summer resulted in a dramatic delay in the initiation of the phytoplankton bloom in some regions and no bloom at all in others. In Region 5, the phytoplankton bloom was delayed by approximately two months due to abnormally extensive sea ice cover. As a result of the reduced length of the growing season, peak Chl *a* concentrations in this region reached only about 50% of normal values (Figure 3b). Unlike most years when the decline of the phytoplankton bloom is precipitated well in advance of ice freeze-up, the rapid drop in Chl *a* and primary production observed in many regions (e.g. Region 5) in 2000–2001 (Figures 3b and 3c) was due to a reduced ice-free growth season (Figure 3a).

[11] The extensive sea ice cover and delayed phytoplankton bloom in 2000–2001 resulted in a substantial drop in the annual phytoplankton production estimated for all regions of the Ross Sea, the severity of which varied spatially. The effect was most extreme in Region 3, where unusually high sea ice cover and an extremely short growing season (Table 1) reduced annual primary production by 95% (Table 1). Annual production in Regions 4 (dominated by diatoms), 5 and 6, where blooms of the alga *Phaeocystis antarctica* are generally the most intense [*Arrigo et al.*, 1998b; *Arrigo et al.*, 2000], was diminished by 32%, 44%, and 35%, respectively in 2000–2001.

Table 1. Regional Differences in Length of Growing Season[a] and Annual Primary Production in the Southwestern Ross Sea in 1998–1999, 1999–2000, and 2000–2001 by Region

Region	1998–1999		1999–2000		2000–2001		% Change[b]	
	Growing Season (Days)	Primary Production (Tg C)	Growing Season (Days)	Primary Production (Tg C)	Growing Season (Days)	Primary Production (Tg C)	Growing Season	Primary Production
1	83	4.9	91	4.9	80	3.0	−8	−40
2	105	5.1	121	5.5	112	3.7	−1	−31
3	59	2.5	81	4.5	0	0.2	−100	−95
4	77	6.0	76	6.9	48	4.4	−37	−32
5	118	9.5	107	10	59	5.5	−48	−44
6	88	13	93	19	54	10	−39	−35
All		41		51		27		−41

Regions are shown in Figure 1.
[a]Defined as the number of continuous days with <50% sea ice cover.
[b]% Change was calculated as the difference between 2000–2001 and the mean of 1998–1999 and 1999–2000.

Oceanographic observations in Chilean coastal waters between Valdivia and Concepción

Larry P. Atkinson,[1] Arnoldo Valle-Levinson,[1] Dante Figueroa,[2] Ricardo De Pol-Holz,[2] Victor A. Gallardo,[2] Wolfgang Schneider,[2] Jose L. Blanco,[1] and Mike Schmidt[3]

Received 23 May 2001; revised 29 November 2001; accepted 11 December 2001; published 25 July 2002.

[1] The physical oceanography of the biologically productive coastal waters of central Chile (36° to 40°S) is relatively unknown. In December 1998 we made a short exploratory cruise between Valdivia (40°S) and Concepción (37.8°S) taking temperature, salinity, oxygen, and current velocity profiles. Coincident sea surface temperature and color measurements were obtained by satellite. The results showed an area dominated by wind-induced coastal upwelling, river runoff, intrusion of offshore eddies, mixing, and heating. Upwelling centers were found over the shelf at three locations: inshore of Mocha Island, off Valdivia, and off Lavapie Point. At these centers, equatorial subsurface water (ESSW) intrudes into the coastal waters, sometimes affecting the surface waters. Since ESSW has characteristically low-oxygen and high-salinity values, it is easily detected. Off Valdivia, runoff imparts stratification, while farther north, solar heating and reduced mixing may facilitate stratification. In some areas, even strong winds would not destroy the stratification imparted by the advection of buoyancy that occurs during the upwelling process. Strong equatorward currents (>1 m s^{-1}) in the form of an upwelling jet were found off Lavapie Point. This is also the location of an intruding anticyclone. Elsewhere, currents were mainly northward but highly variable because of intrusions from offshore eddies. The sea surface temperature and ocean color images show a complex field of onshore and offshore intrusions combined with the effects of mixing on chlorophyll concentrations. The residence time of upwelled water on the shelf is estimated to be less than 1 week. *INDEX TERMS:* 4279 Oceanography: General: Upwelling and convergences; 4516 Oceanography: Physical: Eastern boundary currents; 4528 Oceanography: Physical: Fronts and jets; *KEYWORDS:* Upwelling; wind; water circulation; eddies; central Chile coast

1. Introduction

[2] The coastal waters of Chile are unique because a combination of meteorological and oceanographic processes and geography has created one of the world's most biologically productive ocean areas. The coast extends in a nearly north/south direction over 40° of latitude (not including the Antarctic) bordered by the Andes to the east and the Peru-Chile Trench to the west. Thus Chilean coastal waters lie between two of the highest relief features on Earth. Over this vast latitudinal range, climatic conditions vary from arid to subantarctic with upwelling winds off northern Chile, downwelling winds off southern Chile, and strong westerlies and considerable variability between. Rainfall toward the north is in some places nonexistent, while farther south it is quite high. The extremely high productivity of the Chilean coastal waters is attributable to upwelling of nutrient rich Peru-Chile Undercurrent water [*Strub et al.*, 1998] and processes that maintain biological populations in the shallow coastal waters.

[3] In December 1998 we made an exploratory cruise along the coast between Valdivia (40°S) and Concepción (37.8°S). This region is noted for its extremely high biological productivity that sometimes provides 4% of the world's fish catch. Our preliminary results, based on a unique but sparse data set, show the structure of currents, upwelling centers, and low-salinity water along the coast and the relationship to satellite-derived SST and chlorophyll.

[1]Old Dominion University, Norfolk, Virginia, USA.
[2]University of Concepción, Concepción, Chile.
[3]Goddard Space Flight Center, NASA, Greenbelt, Maryland,

2. Regional Setting

[4] The region studied has a broad shelf that gradually narrows to the north at Lavapie Point (Figure 1). The shelf is about 50 km wide south of Tucapel Point with Mocha Island lying on the outer shelf marking the widest and shallowest part of the shelf. North of Tucapel Point the shelf narrows to about 10 km then starts to widen again at Lavapie Point. The broad and shallow Gulf of Arauco lies northeast of Lavapie Point. The Gulf of Arauco is a large embayment with Santa Maria Island lying offshore inline with the coast to the south. The Bio Bio River flows into the northern end of the Gulf, and the submarine canyon associated with the Bio Bio River crosses the shelf west of its present mouth.

[5] It is important to note two geographic features that affect the wind field. The first feature is change in coastline direction at Lavapie Point. South of Lavapie Point the coastline trends toward 355°T, while north of Lavapie Point

the shore trends toward 20°T. The Gulf of Arauco itself represents a large-scale equatorward facing embayment in the 20°T trending coast. Response to upwelling winds depends on the changing trends of the general bathymetry that follows the shoreline. The changing shoreline direction and diverging isobaths at Lavapie Point would induce upwelling in a northward flowing current [*Arthur*, 1965; *Blanton et al.*, 1981].

[6] The coastal wind field may also be affected by the presence of a coastal range of mountains extending from Concepción southward to the latitude of Mocha Island: the Cordillera de Nahuelbuta. North and south of the Cordillera de Nahuelbuta the coastal range is relatively low in relief. However, maximum heights in the range reach over 1000 m. These heights may cause intensified winds in the adjacent coastal waters.

[7] River flow into the region consists of the Bio Bio River (36.8°S) to the north and the Imperial River (38.8°S), Tolten River (39.2°S), Queule River (39.6°S), and the Calle Calle River (39.8°S) to the south. The previously mentioned cordillera blocks westward flowing rivers in the central part of the region. The total flow in the region from 37° to 40°S is about 3100 m^3 s^{-1} or 100 km^3 yr^{-1} [*Davila et al.*, 2000]. This amount of flow is not large but would be expected to produce areas of low salinity and coastal currents for a few tens of kilometers around the river mouths during the rainy winter season and early summer when the snow melts. South of 40°S the river flow increases significantly relative to flow to the north.

[8] The water mass and general circulation characteristics off central Chile were recently summarized [*Strub et al.*, 1998], so we will keep the review here to a minimum. Wind-driven coastal upwelling is the dominant process in the area during the summer. The cold, salty, nutrient-rich, oxygen-poor equatorial subsurface water (ESSW) flowing southward in the Peru-Chile Undercurrent upwells across the shelf and often intrudes to the coast [*Gunther*, 1936; *Silva and Neshyba*, 1979].

[9] Satellite-derived sea surface temperature imagery [*Cáceres*, 1992] shows filaments and offshore eddies in the region. Offshore anticyclonic eddies are most often found north of Lavapie Point. Offshore-flowing filaments are concentrated in the region just north of Mocha Island and off the Gulf of Arauco. Our data show that offshore and onshore flow affects the inshore waters that we sampled.

3. Methods

[10] In this section we review the methods used and sources of data. The observations were made from the R/V *Kay Kay* operated by the Universidad de Concepción. Between 8 and 11 December 1998 the ship was taken along a path up the coast in a pattern dictated by the schedule and weather (Figure 1). Courses were laid out to sample the coastal current, upwelling centers, and other features of the region. Along the route, continuous current profiles were made with acoustic Doppler current profiler (ADCP) and conductivity-temperature-depth (CTD) casts were made at the end points of each zigzag leg.

[11] Mean monthly upwelling winds were obtained from the NOAA Pacific Fisheries Environmental Laboratory in Monterey, California. We used data from the 36°S node. Coastal winds were obtained from a station at Lavapie Point maintained by the Department of Physics of the Atmosphere and Ocean at the University of Concepción. There are no other wind observations in the region's coastal waters for this time period. Sea surface temperature data were from advanced very high resolution radiometer for 9 December 1998. Images for 10 and 11 December were contaminated with clouds but suggested surface warming consistent with the decreasing upwelling wind speeds. A SeaWifs image from 9 December 1998 was processed using the most recent algorithms for coastal waters.

[12] An RD Instruments Workhorse (300 kHz) ADCP was used to make the current velocity profiles. The ADCP was mounted on a 1.2-m-long catamaran towed several meters to the side of the ship. Raw data were averaged over 90 s and 1-m bins. Bottom tracking was always on, and navigation was by GPS. The data were not detided as the onshore offshore cruise track created nodes similar to tidal nodes if any were present. This was the first time an ADCP was used in this region of Chile.

[13] Temperature, oxygen and salinity profiles were made with a SeaBird 19 CTD. All data where processed using SeaBird software.

4. Results

[14] In this section the results of the observations and other ancillary data are described. First the winds and remotely sensed data are presented, followed by the subsurface observations.

[15] The mean monthly upwelling index (Figure 2a) was very high in late 1998 relative to other years. The short-term record (Figure 2b) shows that the upwelling during the year started in July 1998 and had reached very high values by December. It is clear that our sampling took place during a period of steadily increasing upwelling on the monthly scale. Data from Lavapie Point (Figure 3) indicate a pulse of strong upwelling winds late on 9 December then two smaller events on 10–11 December. The consistent wind stresses over 0.1 N m^{-2} no doubt led to the upwelling we observed, and the decreasing stress on the 10 and 11 December would have caused a decrease in wind-induced upwelling. It should be noted that the cruise was toward the end of an El Niño period and at the beginning of a La Niña.

6. Conclusions

[45] Our limited observations between Valdivia and Concepción during upwelling wind conditions suggest a coastal area strongly influenced by both local upwelling centers and the presence of offshore eddies. That, combined with the influx of runoff into some parts of the region and variations in heating and mixing, creates variations in stratification.

[46] This unique combination of forces and geography result in a complex physical oceanographic situation that apparently results in extremely high biological productivity. Regions such as this one are excellent examples of how carbon, fixed in a coastal upwelling system, is exported offshore. The highly productive fisheries suggest that much of the primary production makes its way to higher trophic levels, but it eventually must be deposited in slope and trench sediments. Examination of those sediments might yield new insights into coastal upwelling and carbon sequestration processes.

[47] The similarities and differences between this region and the California upwelling regions are striking. It seems that comparative studies would be enlightening.

PERGAMON

Deep-Sea Research I 47 (2002) 637–660

DEEP-SEA RESEARCH
PART I

www.elsevier.com/locate/dsr

Phytoplankton pigment and absorption characteristics along meridional transects in the Atlantic Ocean

R.G. Barlow[a,*], J. Aiken[b], P.M. Holligan[c], D.G. Cummings[b], S. Maritorena[d], S. Hooker[e]

[a] *Marine and Coastal Management, Private Bag X2, Rogge Bay 8012, Cape Town, South Africa*
[b] *Plymouth Marine Laboratory, Prospect Place, West Hoe, Plymouth PL1 3DH, UK*
[c] *Southampton Oceanography Centre, Empress Dock, Southampton SO14 3ZH, UK*
[d] *ICESS, University of California, Santa Barbara, CA, USA*
[e] *NASA Goddard Space Flight Centre, Greenbelt, MD 20771, USA*

Received 22 January 2001; received in revised form 12 September 2001; accepted 15 October 2001

Abstract

Pigment patterns and associated absorption properties of phytoplankton were investigated in the euphotic zone along two meridional transects in the Atlantic Ocean, between the UK and the Falkland Islands, and between South Africa and the UK. Total chlorophyll *a* (TChla = MVChla + DVChla + chlorophyllide *a*) concentrations and the biomarker pigments for diatoms (fucoxanthin), nanoflagellates and cyanobacteria (zeaxanthin) appeared to have similar distribution patterns in the spring and in the autumn in the temperate NE Atlantic and the northern oligotrophic gyre. Divinyl chlorophyll *a* levels (prochlorophytes) were greater in spring at the deep chlorophyll maximum in the oligotrophic gyre, however. Marked seasonal differences were observed in the NW African upwelling region. TChla concentrations were twice as high in the upper mixed layer in the spring, with the community dominated by diatoms and prymnesiophytes (19′-hexanoyloxyfucoxanthin). A layered structure was prevalent in the autumn where cyanobacteria, diatoms and prymnesiophytes were located in the upper water column and diatoms and mixed nanoflagellates at the sub-surface maximum. In the South Atlantic, the Benguela upwelling ecosystem and the Brazil-Falklands Current Confluence Zone (BFCCZ) were the most productive regions with the TChla levels being twice as high in the Benguela. Diatoms dominated the Benguela system, while nanoflagellates were the most ubiquitous group in the BFCCZ. Pigment concentrations were greater along the eastern boundary of the southern oligotrophic gyre and distributed at shallower depths. Deep chlorophyll maxima were a feature of the western boundary oligotrophic waters, and cyanobacteria tended to dominate the upper water column along both transects with a mixed group of nanoflagellates at the chlorophyll maximum.

Absorption coefficients were estimated from spectra reconstructed from pigment data. Although absorption was greater in the productive areas, the TChla-specific coefficients were higher in oligotrophic regions. In communities that were dominated by diatoms or nanoflagellates, pigment absorption was generally uniform with depth and attenuating irradiance, with TChla being the major absorbing pigment at 440 nm and photosynthetic carotenoids (PSC) at 490 nm. Absorption by chlorophyll *c* and photoprotective carotenoids (PPC) was much lower. Populations where cyanobacteria were prevalent were characterized by high PPC absorption, particularly at 490 nm, throughout most of the euphotic zone. The data suggested that the effect of pigments on the variability of phytoplankton absorption was due primarily to the variations in absorption by PPC.

1. Introduction

Spatially extensive investigations have been coordinated within the UK Atlantic Meridional Transect (AMT) programme with the purpose of improving our knowledge of biogeochemical processes, ecosystem dynamics and food webs across basin scales in the Atlantic Ocean (Aiken et al., 2000). One of the goals of the programme has been to examine and characterize the properties of biogeochemical provinces (Longhurst et al., 1995), and an objective method was developed to determine the boundaries of physical provinces (Hooker et al., 2000). Another objective has been to conduct ground-truthing measurements of optical and pigment parameters for the validation and calibration of SeaWiFS ocean colour data (Hooker and McClain, 2000). In this regard, the surface distribution pattern of pigments for

transects between the UK and the Falkland Islands was discussed by Gibb et al. (2000), and Barlow et al. (in press) have examined the bio-optical properties of surface pigments in relation to ocean colour data of absorption and back scattering for a transect between South Africa and the UK. Observations of the variability in the vertical distribution of phytoplankton pigments and associated absorption properties across Atlantic basins, however, have not yet been reported.

Total chlorophyll *a* (TChla), defined as the sum of MVChla, DVChla and chlorophyllide *a*, is used as a surrogate marker for the abundance of phytoplankton in the oceans, but other accessory pigments that can be identified and quantified by liquid chromatography (Jeffrey et al., 1997) provide chemotaxonomic information on the range of phytoplankton groups that make up the community structure in the Atlantic (Barlow et al., 1993, in press; Bidigare et al., 1990a; Gibb et al., 2000). The major role of chlorophyll *a* is to absorb light for photosynthesis, but there is also a range of pigments, such as, chlorophylls *b* and *c* plus a variety of carotenoids, that have a significant function in extending the light-harvesting spectrum in the phytoplankton, thus ensuring optimal absorption efficiencies (Kirk, 1994). Other carotenoids, however, serve to protect microalgal cells against the effects of high irradiances, which may damage the photosynthetic apparatus, and these pigments may be termed photoprotective carotenoids (PPC) (Kirk, 1994).

4. Discussion

4.1. Phytoplankton communities

The AMT cruises were essentially confined to investigating only the autumn and spring seasons in the Atlantic because of the logistical programme of the research vessel (Aiken et al., 2000). During AMT-3 (September–October 1996), it was autumn in the North Atlantic and spring in the south; for AMT-6 (May–June 1998), it was autumn in the South Atlantic and spring in the north. Thus, for the NE Atlantic, the two seasons can be compared because the cruise tracks were similar (Fig. 1). The cruise tracks in the southern hemisphere were on opposite sides of the South Atlantic basin, and therefore, the communities along the eastern and western boundaries could be compared, even though the observations were made in different seasons.

The phytoplankton in the temperate NE Atlantic and the northern oligotrophic gyre appeared to have similar characteristics for both the autumn and spring seasons. TChla levels were similar (Figs. 2 and 3) as well as the distribution pattern for diatoms (Fuc) and nanoflagellates (Hex + But + All + Chlb). Dinoflagellates (Per) were detected only in the upper water column on the European shelf during autumn (Fig. 2), but were virtually undetectable in the spring (Fig. 3). The cyanobacterial pattern (Zea) also appeared to be similar for both seasons, although the concentrations of divinyl chlorophyll *a* (prochlorophytes) were greater in the spring (AMT-6) at the deep chlorophyll maxima in the oligotrophic gyre (Figs. 2 and 3). The selected vertical profiles confirmed the observations of the contoured data, but provided more detail on subtle differences. The profiles for 49.68°N and 48.45°N indicated a more diverse nanoflagellate community in the temperate NE Atlantic during autumn (AMT-3) compared to the spring (AMT-6), with chlorophyll *b* being significant in autumn but not in the spring (Figs. 4 and 7). At 29.49°N and 28.68°N, both communities displayed a layered structure, typical of oligotrophic communities, where cyanobacteria (Zea) and prymnesiophytes (Hex) dominated the upper 80–100 m, and a group of mixed flagellates were abundant at the chlorophyll maximum and below (Figs. 4 and 7). Chlorophyll *b* was most prominent at the deep maximum during both seasons, and this was due to the increased synthesis of divinyl chlorophyll *b* in prochlorophyte cells at depth to maximize their absorption of low intensity blue light (Fig. 7, 28.68°N).

These observations are consistent with other studies in the North Atlantic. Bidigare et al. (1990a) and Barlow et al. (1993) reported diatom dominance during spring bloom investigations that were conducted early in the season, followed by a succession to nanoflagellates when key nutrients declined. The temperate NE Atlantic in June 1998 corresponded to the end of bloom conditions, so nanoflagellates were the dominant organisms. The phytoplankton pattern in the northern oligotrophic region appears to be consistent during all seasons, because a similar layering structure of pigments has been demonstrated in North Atlantic oligotrophic waters by Claustre and Marty (1995), Babin et al. (1996), Lazzara et al. (1996) and Goericke (1998). Barlow et al. (in press) and Gibb et al. (2000) estimated the contribution of divinyl chlorophyll *a* to TChla in the northern gyre can be up to 50% in surface waters, indicating the importance of prochlorophytes. Divinyl chlorophyll *a* concentrations in this study were greater at the subsurface maximum than at the surface, but accounted for similar proportions at 37–53% for AMT-3 and 31–50% for AMT-6.

Phytoplankton Productivity

Carbon Assimilation in Marine and Freshwater Ecosystems

Edited by

Peter J. le B. Williams,* David N. Thomas* and Colin S. Reynolds**

*School of Ocean Sciences, University of Wales, Bangor, UK
**Centre for Ecology and Hydrology, Windermere, UK

Blackwell Science

Chapter 7

Assessment of Primary Production at the Global Scale

Michael J. Behrenfeld, Wayne E. Esaias and Kevin R. Turpie

7.1 Introduction

Since the evolution of the first photosynthetic organisms some 3.8 billion years before present (Schopf, 1983), photoautotrophic organisms and the communities they support have continuously altered the chemical composition of the oceans and, through exchange across the air–sea interface, influenced the composition of the overlying atmosphere. Variations in the concentration of radiatively sensitive gases in the atmosphere (e.g. CO_2, CH_4), in turn, influence global climate and consequently ocean circulation, stratification, and the transport of dust to remote ocean regions. These physical forcings govern spatio–temporal variability in phytoplankton distributions through the direct effect of temperature on growth and through their secondary influence on factors such as mixed-layer light availability and the distribution of macro- and micro-nutrients. Perhaps beyond any other observations, satellite measurements of global phytoplankton pigment concentrations have most clearly demonstrated this dependence of ocean productivity on physical processes.

Biogeochemical cycles in the oceans are clearly not in steady state (Falkowski *et al.*, 1998). Biological responses to global perturbations in the physical environment are delayed by the buffering effects of ecosystem complexity. An urgency to characterise such physical–biological feedbacks developed during the final decades of the twentieth century due to escalating public and scientific concerns that environmental impacts of human activities were transitioning from the local to the global scale. At the forefront of these emergent global issues is the potential for a change in climate resulting from rising atmospheric concentrations of carbon dioxide and other 'greenhouse' gases. Unquestionably, sequestration of CO_2 by the photosynthetic biosphere (land and oceans) will play a critical role in future climate trends, but quantifying this CO_2 exchange and its temporal sign remains an uncertainty in global climate models (GCMs).

The most accurately constrained carbon fluxes in GCMs are the release from fossil fuel combustion (presently, $5.5 \pm 0.5 \times 10^{15}$ g C $y^{-1} = 5.5$ petagrams (Pg) y^{-1}) and atmospheric CO_2 accumulation (3.3 ± 0.2 Pg C y^{-1}). Less well quantified is the

terrestrial carbon source from land-use change and deforestation, estimated at 1.6 ± 1.0 Pg C y^{-1} (Sarmiento and Wofsy, 1999). Thus, of the 7.1 Pg C released annually, 3.3 Pg C y^{-1} are retained in the atmosphere and the remaining 3.8 Pg C are removed both abiotically and through photosynthetic fixation. Based on ≈ 2 million measurements of the partial pressure of CO_2 over the oceans (pCO_2) collected across 25 years, the annual oceanic sink for CO_2 has been estimated at 2.0 ± 0.8 Pg C (Sarmiento and Wofsy, 1999). Balancing the global CO_2 budget thus requires an additional sink of 1.8 ± 1.6 Pg C y^{-1}. This 'missing sink' is assumed to involve the biosphere and likely entails both oceanic and terrestrial components. Partitioning of the unaccounted carbon between the land and oceans is difficult, however, because it represents less than 2% of biospheric net primary production, estimated at 111–117 Pg C y^{-1} (Behrenfeld *et al.* 2001a).

7.6 Summary

Primary productivity models, when coupled with time-varying global measurements of phytoplankton biomass, provide critical information for detecting changes in oceanic carbon fluxes. Such models are also beneficial for assessing ecological responses to regional changes in nutrient loading and may provide estimates of biologically mediated long-term carbon sinks if linked to secondary models of export production. The foundation of both aquatic and terrestrial NPP models is similar and, in the simplest terms, can be described as equating NPP to the product of plant biomass and light utilisation efficiency. From this basic relationship, a wide variety of phytoplankton productivity models have developed. At the categorical level, these models differ with respect to the presumed importance of resolving the time, depth, and spectral dependence of photosynthesis. Within each model category, differences largely centre around the specific treatment of the photosynthesis–irradiance relationship and in the characterisation of the underwater light field.

In this chapter, we have attempted to describe the relationship between various NPP models and the assumptions required to progress from fully expanded WRMs to the very simple DIMs. We have argued that all global estimates of NPP are critically dependent on the approach employed for modelling light-saturated photosynthesis and demonstrated this conclusion using two temperature-dependent models and a new light-nutrient model. This later model produces ΣNPP estimates comparable with local-scale, daily ^{14}C-uptake results. Although the model was applied to global satellite C_{sat} data using a simple DIM formulation, its description at the level of chlorophyll synthesis and Calvin cycle reactions is ideally suited for application in a WRM. The primary advantage of using a spectrally resolved model will be the improved estimates of mixed-layer acclimation irradiances, which are a primary forcing factor for variability in P^b_{max}.

Over the 50 year history of productivity modelling, significant advances have been made toward assessing global-scale phytoplankton photosynthesis. Noteworthy accomplishments include the development of variable P^b_{max} models; characterisation of the underwater light field; description of vertical variability in phytoplankton biomass distributions, and the development of remote sensing capabilities that now provide global measurements of near-surface chlorophyll every two days. These achievements notwithstanding, we hope our discussion has impressed upon the reader the need for further improvements in primary productivity modelling. These improvements will require laboratory, field, computational and remote sensing components, all of which represent exciting challenges for future research programmes.

Vol. 228: 103–117, 2002 | MARINE ECOLOGY PROGRESS SERIES
Mar Ecol Prog Ser | Published March 6

Photoacclimation and nutrient-based model of light-saturated photosynthesis for quantifying oceanic primary production

Michael J. Behrenfeld[1,*], Emilio Marañón[2], David A. Siegel[3], Stanford B. Hooker[1]

[1]National Aeronautics and Space Administration, Goddard Space Flight Center, Code 971, Building 33, Greenbelt, Maryland 20771, USA
[2]Departamento de Ecología y Biología Animal, Universidad de Vigo, 36200 Vigo, Spain
[3]Institute for Computational Earth System Science, University of California Santa Barbara, Santa Barbara, California 93106-3060, USA

ABSTRACT: Availability of remotely sensed phytoplankton biomass fields has greatly advanced primary production modeling efforts. However, conversion of near-surface chlorophyll concentrations to carbon fixation rates has been hindered by uncertainties in modeling light-saturated photosynthesis (P^b_{max}). Here, we introduce a physiologically-based model for P^b_{max} that focuses on the effects of photoacclimation and nutrient limitation on relative changes in cellular chlorophyll and CO_2 fixation capacities. This 'PhotoAcc' model describes P^b_{max} as a function of light level at the bottom of the mixed layer or at the depth of interest below the mixed layer. Nutrient status is assessed from the relationship between mixed layer and nutricline depths. Temperature is assumed to have no direct influence on P^b_{max} above 5°C. The PhotoAcc model was parameterized using photosynthesis-irradiance observations made from extended transects across the Atlantic Ocean. Model performance was validated independently using time-series observations from the Sargasso Sea. The PhotoAcc model accounted for 70 to 80% of the variance in light-saturated photosynthesis. Previously described temperature-dependent models did not account for a significant fraction of the variance in P^b_{max} for our test data sets.

KEY WORDS: Photosynthesis · Modeling · Primary production

INTRODUCTION

Photosynthesis is a fundamental process of nearly all known ecosystems, such that the level of photoautotrophic carbon fixation supported by a given environment broadly dictates the local biomass of subsequent trophic levels and the biogeochemical exchange of elements between systems. Models of biospheric primary production have been greatly aided by global-scale satellite observations (Field et al. 1998), but conversion of measured plant biomass to net photosynthesis has remained problematic. Whereas terrestrial productivity models suffer from a lack of observational data for parameterization and testing (Field et al. 1998), high-sensitivity measurements of net primary production in aquatic systems have been routine since the introduction of the ^{14}C method by Steemann Nielsen (1952).

Analyses of vertical profiles of phytoplankton photosynthesis revealed early on that, when normalized to depth-specific chlorophyll concentrations, primary production can be modeled to first order simply as a function of subsurface irradiance (Ryther 1956, Ryther & Yentsch 1957, Talling 1957). A variety of analytical expressions have consequently been developed de-

scribing this relationship between vertical light attenuation and chlorophyll-normalized carbon fixation (reviewed by Platt & Sathyendranath 1993, Behrenfeld & Falkowski 1997b). Such models can account for most of the observed variance in depth-integrated photosynthesis (ΣPP), particularly when measurements encompass a wide phytoplankton biomass range, provided model input includes measured values for: (1) the vertical distribution of chlorophyll, (2) the downwelling attenuation coefficient (K_d) for photosynthetically active radiation (PAR), and (3) the maximum carbon fixation rate per unit of chlorophyll (P^b_{opt}) (Behrenfeld & Falkowski 1997a,b).

For over 40 yr, developments in phytoplankton primary production models have focused on refining characterizations of the above 3 critical water-column features, with clearly the greatest achievements realized in the description of the underwater light field (e.g. Platt & Sathyendranath 1988, Morel 1991, Antoine et al. 1996). Progress has also been made in predicting vertical profiles of chlorophyll (Platt & Sathyendranath 1988, Morel & Berthon 1989), but models of P^b_{opt} have remained rudimentary and inconsistent (Behrenfeld & Falkowski 1997b). The importance of accurate P^b_{opt} estimates cannot be overstated, especially when model performance is evaluated by comparison with point-source field observations. For globally representative data sets, phytoplankton biomass alone accounts for <40% of ΣPP variability, while inclusion of measured P^b_{opt} values can account for >80% of the variance in ΣPP (Balch & Byrne 1994, Behrenfeld & Falkowski 1997a). In oligotrophic regions where the range in chlorophyll concentration is further constrained, accurate estimates of P^b_{opt} are even more critical (Banse & Yong 1990, Siegel et al. 2000).

The function of P^b_{opt} models is to capture spatial and temporal changes in assimilation efficiencies (i.e. carbon fixed per unit of chlorophyll) resulting from physiological acclimation to environmental variability. Currently, the 2 principal approaches for estimating P^b_{opt} in regional- to global-scale models are: (1) to assign fixed, climatological values to biogeographical provinces (Longhurst 1995, Longhurst et al. 1995), and (2) to define predictive relationships between P^b_{opt} and 1 or more environmental variables (e.g. temperature, nutrient concentration) (Megard 1972, Balch et al. 1992, Antoine et al. 1996, Behrenfeld & Falkowski 1997a). Both techniques have advantages, but differ in their intended application. For example, the first approach furnishes broad-scale average values for designated regions and is not intended to accurately reproduce the much finer scale physiological variability in ^{14}C-uptake rates corresponding to a given day, depth and location. As for the second approach, an effective model should, ideally, provide P^b_{opt} estimates comparable at this point-source scale of field measurements, but a successful model of this genre has not yet been described.

Here we introduce a model, belonging to this second category, that captures P^b_{opt} variability in natural phytoplankton assemblages. The model largely focuses on changes in P^b_{opt} resulting from photoacclimation and is thus referred to as the 'PhotoAcc Model', although a nutrient-dependence is also prescribed. In the following section, we describe the conceptual basis and underlying equations of the PhotoAcc model, the field data used for model parameterization and testing, and our approach to assessing nutrient status and photoacclimation irradiances. Model limitations, directions for expansion, and potential avenues for global implementation are addressed in the section 'Discussion'.

DISCUSSION

The importance of effectively modeling light-saturated photosynthesis at the difficult local scale of daily primary production measurements has been recognized for over 40 yr (Ryther 1956, Ryther & Yentsch 1957). The most common approach to this problem has been to describe P^b_{opt} as a function of temperature. Such models capture only a fraction of the observed variability in P^b_{opt}, because temperature is weakly correlated with causative environmental forcing factors. In contrast, the PhotoAcc model attempts to explicitly describe primary causative relationships at the level of chlorophyll synthesis and changes in the Calvin cycle capacity. With this approach, the model effectively reproduced spatial and temporal variability in light-saturated photosynthesis for the AMT and BATS studies. These field programs do not, however, fully encompass global nutrient, light, and temperature conditions. In the following sections, we evaluate the predictions and hypotheses of the PhotoAcc model, discuss potential alterations to account for additional growth constraints, and propose avenues for global implementation.

Decadal changes in global ocean chlorophyll

Watson W. Gregg
Laboratory for Hydrospheric Processes, NASA/Goddard Space Flight Center, Greenbelt, Maryland, USA

Margarita E. Conkright
Ocean Climate Laboratory, NOAA/National Oceanographic Data Center, Silver Spring, Maryland, USA

Received 8 January 2002; accepted 24 April 2002; published 7 August 2002.

[1] The global ocean chlorophyll archive produced by the CZCS was revised using compatible algorithms with SeaWiFS. Both archives were then blended with in situ data to reduce residual errors. This methodology permitted a quantitative comparison of decadal changes in global ocean chlorophyll from the CZCS (1979–1986) and SeaWiFS (1997–2000) records. Global spatial distributions and seasonal variability of ocean chlorophyll were similar, but global means decreased over the two observational segments. Major changes were observed regionally: chlorophyll concentrations decreased in the northern high latitudes while chlorophyll in the low latitudes increased. Mid-ocean gyres exhibited limited changes. The overall spatial and seasonal similarity of the two data records suggests that the changes are due to natural variability. These results provide evidence of how the Earth's climate may be changing and how ocean biota respond. *INDEX TERMS:* 1620 Global Change: Climate dynamics (3309); 4805 Oceanography: Biological and Chemical: Biogeochemical cycles (1615); 4215 Oceanography: General: Climate and interannual variability (3309); 1635 Global Change: Oceans (4203); 4275 Oceanography: General: Remote sensing and electromagnetic processes (0689)

1. Introduction

[2] The Sea-viewing Wide Field-of-view Sensor (SeaWiFS) has produced the first multi-year time series of global ocean chlorophyll observations since the demise of the Coastal Zone Color Scanner (CZCS) in 1986. Global observations from 1997–2000 by SeaWiFS combined with observations from 1979–1986 by the CZCS should in principle provide an opportunity to observe decadal changes in global ocean chlorophyll. However, incompatibilities between algorithms have so far precluded quantitative analysis. We have developed and applied compatible processing methods for the CZCS [*Gregg et al.*, 2002], using recent advances in atmospheric correction and consistent bio-optical algorithms to enhance the CZCS archive to comparable quality with SeaWiFS. Even with careful application of modern methodologies, there remain residual errors deriving from assumptions of atmospheric and oceanic optical behavior. We applied blending methodologies [*Gregg and Conkright*, 2001], where in situ data observations are merged with the satellite data, to reduce residual errors. These re-analyzed, blended data records provide maximum compatibility and permit, for the first time, a quantitative analysis of the changes in global ocean chlorophyll from the early-to-mid 1980's to the present.

2. Methods

[3] Reanalyzed CZCS chlorophyll data (Jan 1979–Jun 1986) [*Gregg et al.*, 2002] and Version 3 SeaWiFS data (Sep 1997–Dec 2000) were averaged to produce seasonal means at 1° spatial resolution, and were then blended with in situ chlorophyll data [*Gregg and Conkright*, 2001]. In statistical analyses of these data sets, we excluded comparisons in the North Pacific, North Atlantic, and Antarctic basins poleward of 40° in local autumn and winter, because of sparse sampling by the CZCS. These were the only places and times when the lower density sampling of the CZCS was important in the comparison. Basin and global means were areally-weighted for both satellite data sets and only co-located observations were used, to further minimize problems associated with low sampling density by the CZCS. Coastal observations (where bottom depth $\leq$200 m) were excluded from the analysis.

[4] Sea surface temperature (SST) and surface mean wind stress data were obtained from the NOAA/National Center for Environmental Prediction (NCEP) Reanalysis Project. The data were averaged over the two observational segments corresponding to the CZCS and SeaWiFS. Only data co-located with the ocean color data were used in the means.

3. Global and Basin Scale Decadal Changes in Blended Ocean Chlorophyll

[5] Blended satellite/in situ observations indicated that global ocean chlorophyll has decreased since the CZCS data record (Table 1). The decreases ranged from about 9% in autumn (Oct–Dec) to nearly 11% in summer (Jul–Sep). No significant change was observed in winter (Jan–Mar) or spring (Apr–Jun). Seasonal temporal patterns between the blended satellite chlorophyll records were similar, indicating a global maximum in spring/summer and a minimum in winter/autumn. The annual mean global change was −6.1% from the early 1980's to the present.

[6] Much of the global decrease was due to changes in the high latitudes (Figure 1). Blended SeaWiFS data were more than 10% lower than blended CZCS in the North Pacific and Atlantic basins in summer (Figure 1). The southern mid-ocean basins, South Indian, South Pacific, and South Atlantic, all exhibited significant decreases in blended chlorophyll in spring and summer, to nearly 28% in the South Pacific.

Table 1. Global ocean chlorophyll concentrations (mg m^{-}) and standard deviations from the blended CZCS record (1979–1986) and the modern blended SeaWiFS record (1997–2000), and the percent change (SeaWiFS-CZCS). *An asterisk indicates statistical significance at $P < 0.05$.

	Winter (Jan–Mar)	Spring (Apr–Jun)	Summer (Jul–Sep)	Autumn (Oct–Dec)
CZCS	0.232±0.359	0.250±0.402	0.288±0.431	0.242±0.412
SeaWiFS	0.225±0.309	0.245±0.375	0.257±0.347	0.221±0.296
% difference	−2.8	−2.1	−10.7*	−8.6*

compatibility. The analysis of the two chlorophyll records indicated large similarity in the global spatial distributions and seasonal variability. This included the extent and spatial structure of the mid-ocean gyres, the equatorial upwelling regions, and the bloom-recede dynamics of the high latitudes. There were also many decadal changes indicated in the analysis of the archives. Global chlorophyll concentrations indicated a decrease from the CZCS record to the present, of about −6%. Larger reductions occurred in the northern high latitudes. Conversely, chlorophyll in the low

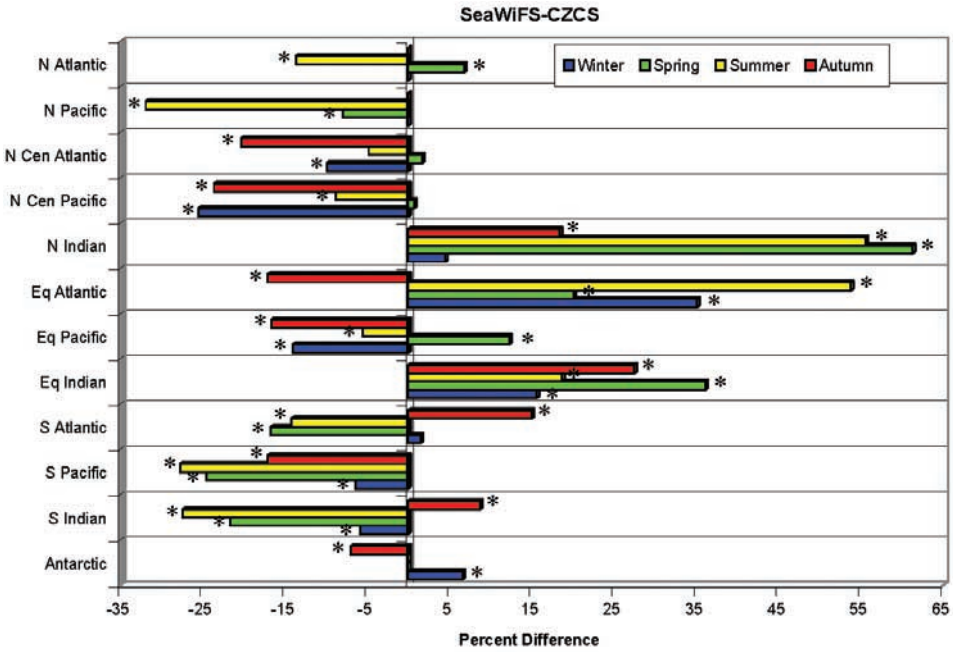

Figure 1. Seasonal differences between blended SeaWiFS and blended CZCS chlorophyll in the 12 major oceanographic basins [*Gregg et al.*, 2002]. Equatorial basins are between −10° and 10° latitude, the North Pacific and North Atlantic are north of 40°, and Antarctic is south of −40°. The other basins fall within these limits. Differences are expressed as blended SeaWiFS-blended CZCS. An asterisk indicates the difference is statistically significant at $P < 0.05$.

[7] The low latitude oceanographic basins, in contrast, generally exhibited an increase in chlorophyll from the CZCS period (Figure 1). Three of these basins (North Indian, Equatorial Indian, Equatorial Atlantic) showed major increases for the blended SeaWiFS. An exception was the equatorial Pacific in winter, summer, and autumn.

5. Summary

[17] The CZCS global ocean chlorophyll archive was reanalyzed using compatible atmospheric correction and bio-optical algorithms with SeaWiFS. This permitted, for the first time, a quantitative comparison of the decadal trends in global ocean chlorophyll from 1979- mid-1986 to the present (Sep 1997–Dec 2000). Blending of both archives with available coincident in situ data improved the residual errors of each data record and provided further latitudes increased. Mid-ocean gyres exhibited limited changes. These results may indicate facets of climate change, some of which may be related to regional oscillation behavior such as the PDO and ENSO. Some of the decadal changes can be attributed to observed changes in SST or meteorological forcing, but some cannot. We believe that this reanalysis of the CZCS and SeaWiFS archives enables identification of some aspects of decadal change, and provides a marker of how the Earth's climate may be changing and how ocean biota respond.